Journal of Applied Electrochemistry (2024) 54:1–11
https://doi.org/10.1007/s10800-023-01955-3

RESEARCH ARTICLE

Synthesis and characterization of CuO micro-flowers/PPy nanowires nanocomposites as high-capacity anode material for lithium-ion batteries

M. Helli[1] · S. K. Sadrnezhaad[1] · S. M. Hosseini-Hosseinabad[1] · P. Vahdatkhah[1]

Received: 6 May 2023 / Accepted: 22 July 2023 / Published online: 7 August 2023

Abstract
A novel set of CuO/PPy nanocomposites (NCs) with varying PPy weight ratios was synthesized via microwave irradiation and oxidative chemical polymerization. The resulting NCs and CuO micro-flowers were characterized by X-ray diffraction, Fourier transform infrared spectroscopy, thermogravimetric analysis, Brunauer–Emmett–Teller analysis, field-emission scanning electron microscopy, energy-dispersive X-ray spectroscopy line, and dot mapping techniques. The formation mechanism of CuO micro-flowers and PPy nanowires were discussed in detail. The electrochemical lithium-ion storage properties of all samples, used as anode materials in Li-ion batteries, were measured. Our results indicate that PPy nanowires with various weight ratios play a critical role in the lithium storage properties of the hybrid CuO/PPy NCs. An increase in the nanowire mass ratio enhances the cyclic durability and charge/discharge capacities of the PPy/CuO NCs. Specifically, NCs containing 3.5-, 5-, 6.2-, and 8.8-wt% PPy nanowires exhibit reversible capacities of 128, 231, 371, and 200 mAh g^{-1}, respectively. The superior performance of the hybrid CuO/PPy NCs is attributed to the PPy nanowires. The CuO/PPy NCs benefit from the nanowire morphology and composite structural features that can accommodate the dramatic volume expansion of CuO during discharge/charge steps and enhance electrical conductivity. Our study demonstrates that tuning the PPy nanowire mass ratio in hybrid Metal Oxide/Polymer NCs is an effective method to enhance the electrode performance of an energy storage device.

✉ S. K. Sadrnezhaad
sadrnezh@sharif.edu

M. Helli
Motahareh.helli.94@gmail.com

[1] Department of Materials Science and Engineering, Sharif University of Technology, Tehran 11365-9466, Iran

Graphical abstract

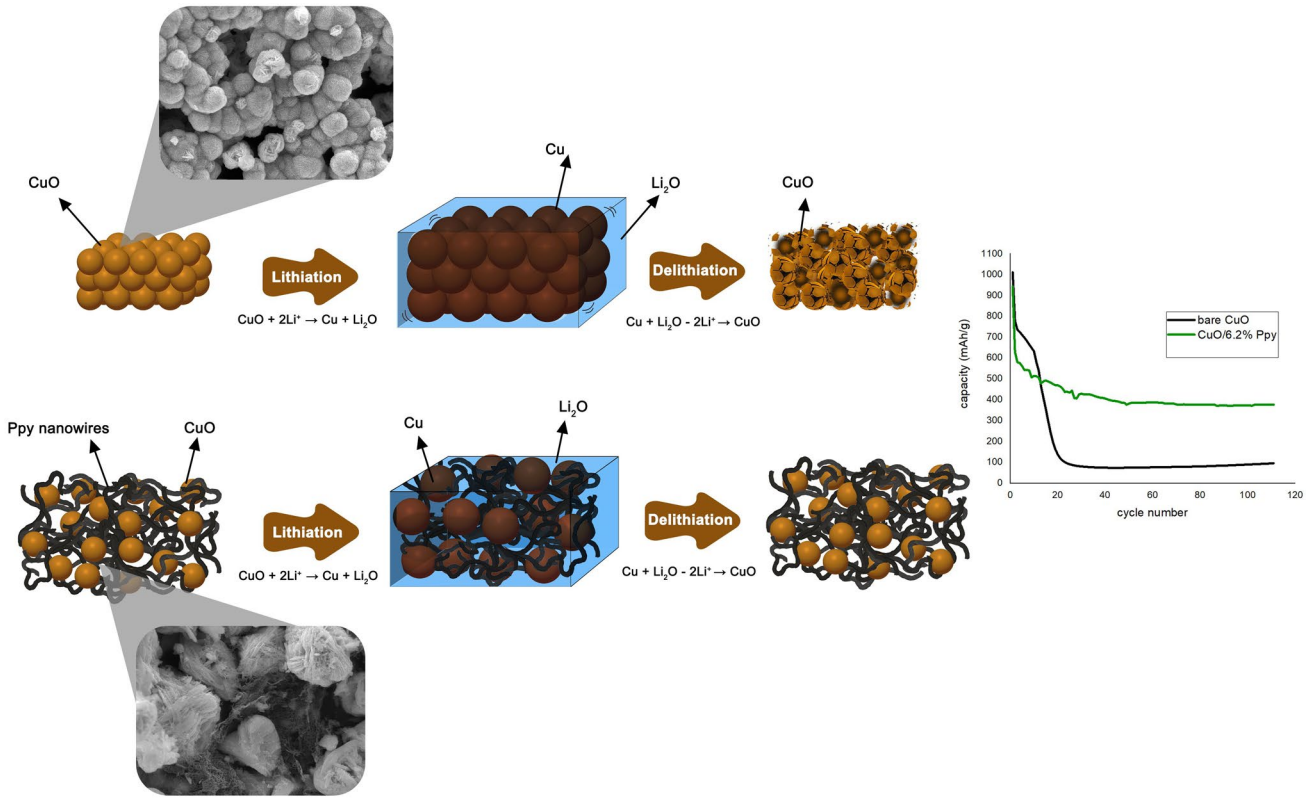

Keywords Li-ion battery · Anode material · Polypyrrole nanowires · CuO micro-flowers · Microwave-assisted synthesis

1 Introduction

In recent decades, the depletion of fossil fuels and environmental problems resulting from increasing greenhouse gas emissions have emerged as some of the most pressing global challenges. Lithium-ion batteries (LIBs) have become a promising alternative to carbon-based fuels, garnering significant attention for their high energy storage capacity and application as power components in various electronic devices, such as electric vehicles, laptops, and mobile phones [1–4]. However, to meet the ever-growing demand for portable energy storage devices, improvements in the electrochemical capacity, cyclic durability, and rate ability of LIBs are necessary. The anode electrode is a crucial component of LIBs that plays a significant role in their electrochemical performance. Among all types of anode materials, transition metal oxides (TMOs) are particularly promising alternatives [5–8]. CuO, in particular, is frequently used as an anode material due to its high electrochemical capacity, abundance, safety, low costs, and environmental friendliness. However, TMOs face several challenges, such as low electrical conductivity and significant volume change during consecutive charge/discharge processes as active anode materials. These problems often cause electrode pulverization, electrical disconnection, and consequent rapid capacity decay, thereby impeding the use of TMOs, including CuO, as anode materials in LIBs [9–12].

Numerous attempts have been made to optimize the size and morphology of CuO particles to overcome the aforementioned issues. To date, nanoparticles with various structures and morphologies, such as wires, tubes, plates, and dots, have been synthesized. Among the synthesized structures, CuO micro-flowers have been found to exhibit high capacity and stability, owing to their large surface area and short lithium-ion diffusion length [13–19]. Another approach to address the challenges of TMOs, such as pulverization and low conductivity, is to enhance their electrochemical properties by introducing organic conducting polymers, such as polyaniline and polypyrrole, as matrices or coating layers. These conducting polymers can accommodate volume changes during consecutive charge and discharge processes, thereby increasing the cyclability of the anode. Furthermore, conducting polymers

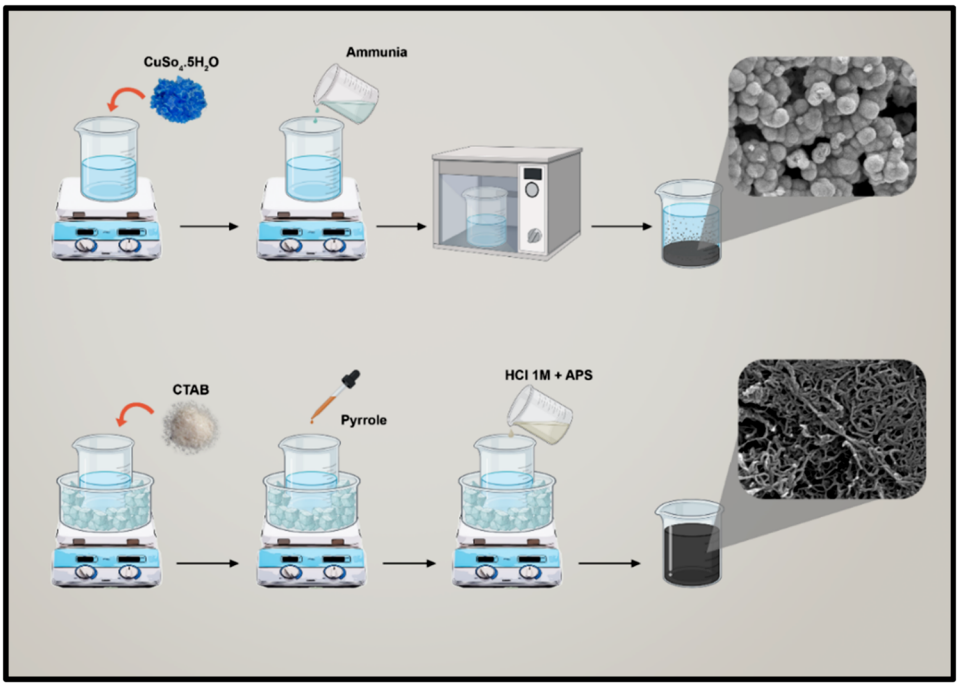

Fig. 1 A schematic of CuO micro-flowers and PPy nanowires synthesis procedure

can improve the conductivity of the active material and enhance electrode charge transfer [20–23].

In prior studies, researchers had developed Core–shell CuO@PPy composites using various techniques and investigated their electrochemical performance as Lithium-ion anode material. For instance, Yin et al. synthesized core–shell CuO nanobelts@PPy and examined their electrochemical properties as anode materials, exploring the influence of PPy shell thickness on the anode's cyclability [24, 25]. In another study, Feng et al. synthesized CuO nanocrystals coated with a PPy shell, utilizing KCl as a dopant to address metal oxide capacity degradation in Lithium-ion anode materials [26]. While previous investigations have employed PPy as a coating layer on CuO particles, we have fabricated novel CuO micro-flower/PPy nanowire nanocomposites (NCs) by synthesizing PPy nanowires. Our study focuses on exploring the influence of PPy nanowires on the electrochemical performance of CuO particles.

2 Experimental section

2.1 Materials

Copper(II) sulfate pentahydrate ($CuSO_4.5H_2O$), ammonia solution 25% (NH_4OH), pyrrole (C_4H_5N, Py), cetyltrimethylammonium bromide ($C_{19}H_{42}BrN$, CTAB), hydrochloric acid (HCl) solution, and anhydrous ethanol were purchased from Merck, and ammonium persulfate ($(NH_4)_2S_2O_8$) were purchased from Tetra-Chem.

2.2 Preparation of samples

2.2.1 Synthesis of CuO micro-flowers

For synthesizing flower-shaped CuO micro-particles, a 1.6×10^{-5} mM solution of Copper(II) sulfate pentahydrate in DI water was prepared by a magnetic stirrer. Then, a proper amount of ammonia 25% was added dropwise to the solution and stirred until reaching a pH of 11.5. Then, the solution was put in a microwave oven and irritated for 30 min at 900W. CuO micro-flower particles were synthesized and precipitated as a black powder (Fig. 1).

2.2.2 Synthesis of PPy nanowire

Polypyrrole nanowire particles were synthesized by the in situ chemical oxidative polymerization method in the presence of cetyltrimethylammonium bromide (CTAB) as template and ammonium persulfate (APS) as oxidant agent. In a typical process, 1.4 gr CTAB (0.1M) was first dissolved in 40-ml HCl (1M) and stirred for 1 h. Afterward, the solution was cooled to 0 °C, then 0.3-ml pre-distilled pyrrole monomer (was distilled and kept against exposure to light to eliminate residual polymerization) was added dropwise and stirred vigorously (1200 rpm). In this step, the viscosity of the solution increased dramatically. Second, the oxidant solution was prepared by dissolution of 0.27 gr APS in 40-ml HCl (1M) and cooled to 0 °C, and then added to the previous solution. The mixture was stirred for 24 h constantly in an ice bath. The achieved black precipitate was filtered and

washed with a copious amount of DI water and ethanol till reaching pH 7 in the resulting suspension (Fig. 1).

To prepare CuO/PPy composites with different PPy weight ratios, a calculated amount of polypyrrole suspension and synthesized CuO micro-flowers were stirred for 2 h. The product was filtered and dried in the oven at 80 °C for 12 h. CuO@PPy nanocomposite with 3.5-, 5-, 6.2-, and 8.8-wt% PPy was prepared and used as anodic active material.

3 Results and discussion

3.1 TGA

Thermogravimetric analysis (TGA) was performed on both bare CuO micro-flowers and CuO/PPy NCs with varying PPy weight ratios in the N_2 atmosphere to quantify the amount of PPy in the nanocomposites. The samples were heated from 25 to 600 °C at a rate of 10 °C min^{-1}. The TGA results are presented in Fig. 2a. The slight weight loss observed in both bare CuO and CuO/PPy NCs samples below 200 °C is likely attributed to the removal of surface hydroxyls or absorbed solvents. The weight loss between 200 and 600 °C in the NCs samples is predominantly due to the decomposition of PPy in the N_2 atmosphere [27, 28]. In contrast, the bare CuO sample shows no significant weight loss in the tested temperature range. Based on the weight loss in the TGA curves, the mass fraction of PPy in the NCs samples was determined to be 3.5%, 5%, 6.2%, and 8.8%.

3.2 XRD

X-ray Diffraction (XRD) analysis was performed to investigate the crystalline structure of the synthesized samples. Figure 2b illustrates the XRD patterns of bare CuO, pure PPy nanowires, and CuO/PPy NCs with varying PPy mass ratios. All the characteristic diffraction peaks of bare CuO and NCs align well with the monoclinic phase of CuO (JCPDS No.05-0661), which exhibits diffraction peaks at 32.5°, 35.6°, 38.8°, 48.8°, 53.4°, 58.2°, 61.6°, 66.3°, and 68.1°, attributed to the (110), ($\bar{1}$11), (111), ($\bar{2}$02), (020), (202), ($\bar{1}$13), ($\bar{3}$11), and (220) planes of the monoclinic structure of CuO [29, 30]. The absence of any impurity diffraction peaks, such as $Cu(OH)_2$ and Cu_2O, confirms the high purity of the synthesized CuO micro-flowers and CuO NCs. Additionally, the pure PPy XRD curve displays a broad peak at $2\theta \sim 23°$, indicating the amorphous structure of PPy. However, this peak is scarcely noticeable in CuO/PPy samples due to its weak intensity in comparison to the CuO diffraction peak [24].

3.3 FT-IR

The chemical structure and composition of the synthesized samples were determined using Fourier transform infrared (FT-IR) spectra. As shown in Fig. 2c, two absorption bands at 497 cm^{-1} and 611 cm^{-1} were observed in all samples, which can be attributed to the Cu–O stretching vibration, indicating the successful formation of monoclinic CuO in the samples. Absorption peaks at 1620 cm^{-1} were identified as existing water molecules in the products. The peak at approximately 1462 cm^{-1} is assigned to the stretching vibration of the C–N bond in the PPy ring, while peaks near 1065 cm^{-1} and 789 cm^{-1} are ascribed to the C–H in-plane and out-of-plane vibrations in the PPy ring, respectively [31, 32].

3.4 BET

The Brunauer–Emmett–Teller (BET) gas-sorptometry technique was employed to determine pore volume, pore diameter, and specific surface area of the as-prepared CuO micro-flowers, as shown in Fig. 3. The N_2 adsorption/desorption isotherms of the synthesized CuO micro-flowers exhibited the typical type IV behavior, which is indicative of mesoporous materials and is characterized by the presence of a hysteresis loop [33]. The BET specific surface area of the synthesized CuO micro-flowers was determined to be 14.504 $m^2\ g^{-1}$, while the single point adsorption total pore volume was found to be 0.047757 $cm^3\ g^{-1}$. Additionally, analysis of the corresponding Barrett–Joyner–Halenda (BJH) pore diameter distribution curve revealed an average pore size of 13.171 nm.

3.5 Morphology

The present study employed field-emission scanning electron microscopy (FESEM), EDS, and EDX to analyze the morphology, size, and chemical composition of bare CuO particles, PPy nanowires, and CuO/PPy NCs. As demonstrated in Fig. 4, CuO particles exhibit uniform micro-flowers consisting of intermingled ultrathin nanosheets, forming hierarchical nanostructures with a relatively large surface area. This unique structure has been shown to reduce the diffusion length of lithium ions and improve lithium storage. To synthesize CuO micro-flowers, Copper(II) sulfate was employed as a Cu precursor in alkaline aqueous media with the addition of ammonia to increase the solution's pH. The reaction between Cu^{2+} and NH_4OH led to the formation of $Cu(OH)_2$ precipitates as initial nuclei. Upon microwave irradiation of the solution for 30 min at 900 W, CuO nanoflakes were produced, as indicated by reaction 2.

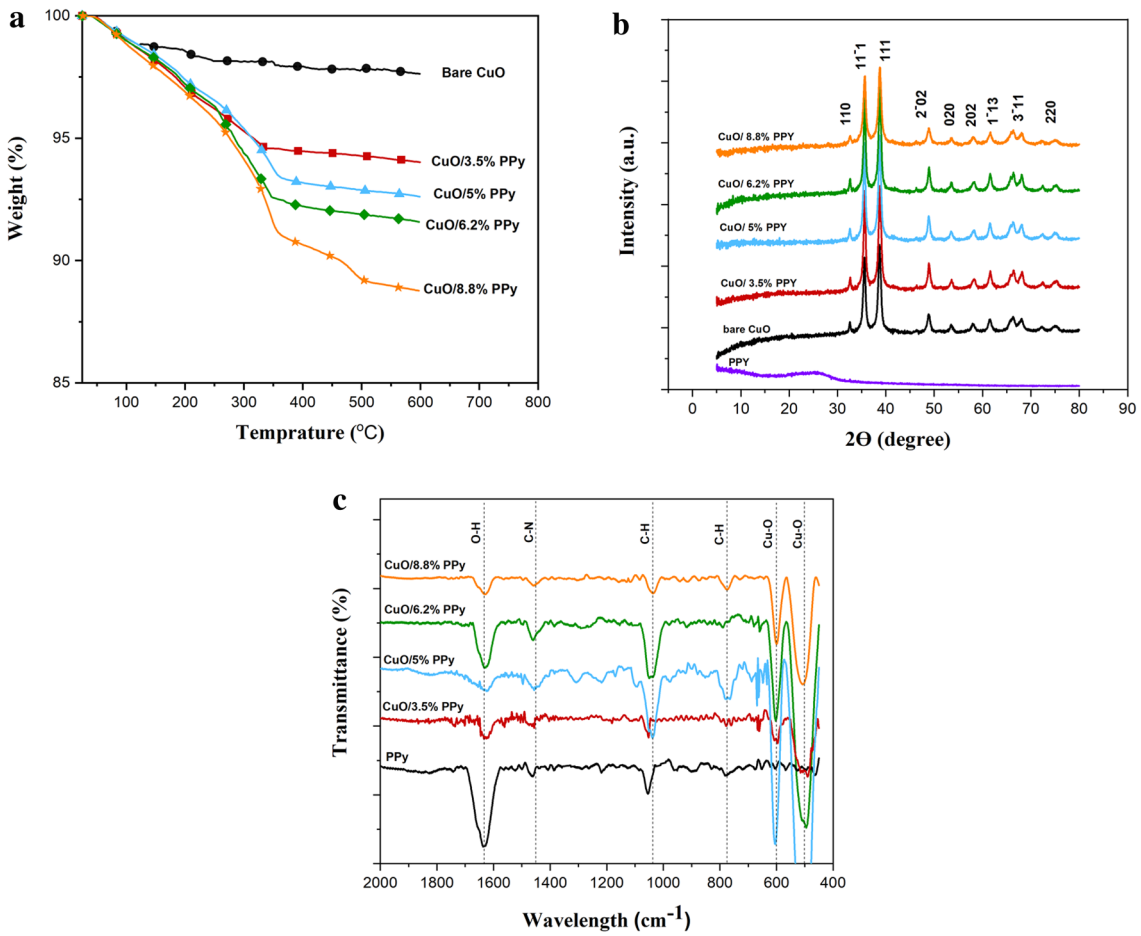

Fig. 2 TGA (**a**), XRD (**b**), and FT-IR (**c**) curves of bare CuO micro-flowers and CuO/PPy NCs with different PPy weight ratios. CuO/PPy NCs synthesized with different polymerization times

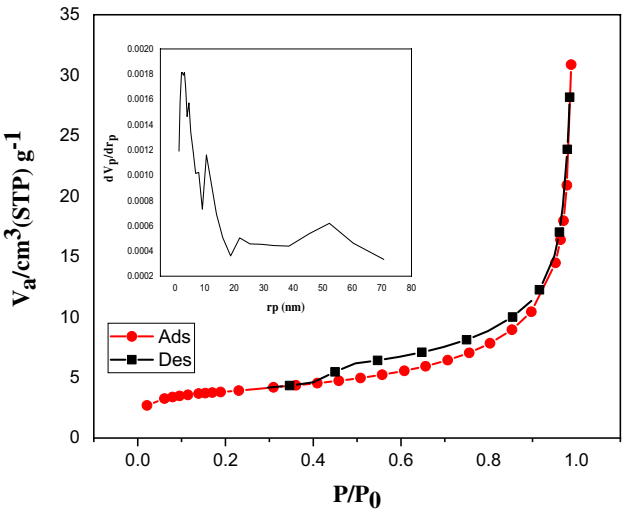

Fig. 3 N2 adsorption–desorption isotherms and the pore size distribution of the CuO micro-flowers

$$Cu^{2+} + 2NH_4OH \rightarrow Cu(OH)_2 \downarrow + 2NH^{4+} \quad (1)$$

$$Cu(OH)_2(s) \xrightarrow{\Delta} CuO\ (s) + H_2O\ (l) \quad (2)$$

It is noteworthy that the presence of excess NH_3 and NH_4 in the solution may dissolve $Cu(OH)_2$ precipitates, resulting in the formation of CuO particles via the complex reaction shown below:

$$Cu(OH)_2 + 4NH_3 + 2NH^{4+} \rightarrow \left[Cu\left(NH_3\right)_4\right]^{2+} + 2NH_3.H_2O \quad (3)$$

$$\left[Cu\left(NH_3\right)_4\right]^{2+} + 2OH \rightarrow CuO(s) + 4NH_3 + H_2O(l) \quad (4)$$

Therefore, it is essential to optimize the ammonia concentration to synthesize CuO nanoflakes successfully. A high ammonia concentration may lead to the dissolution of $Cu(OH)_2$ precipitates, preventing the formation of CuO particles [15].

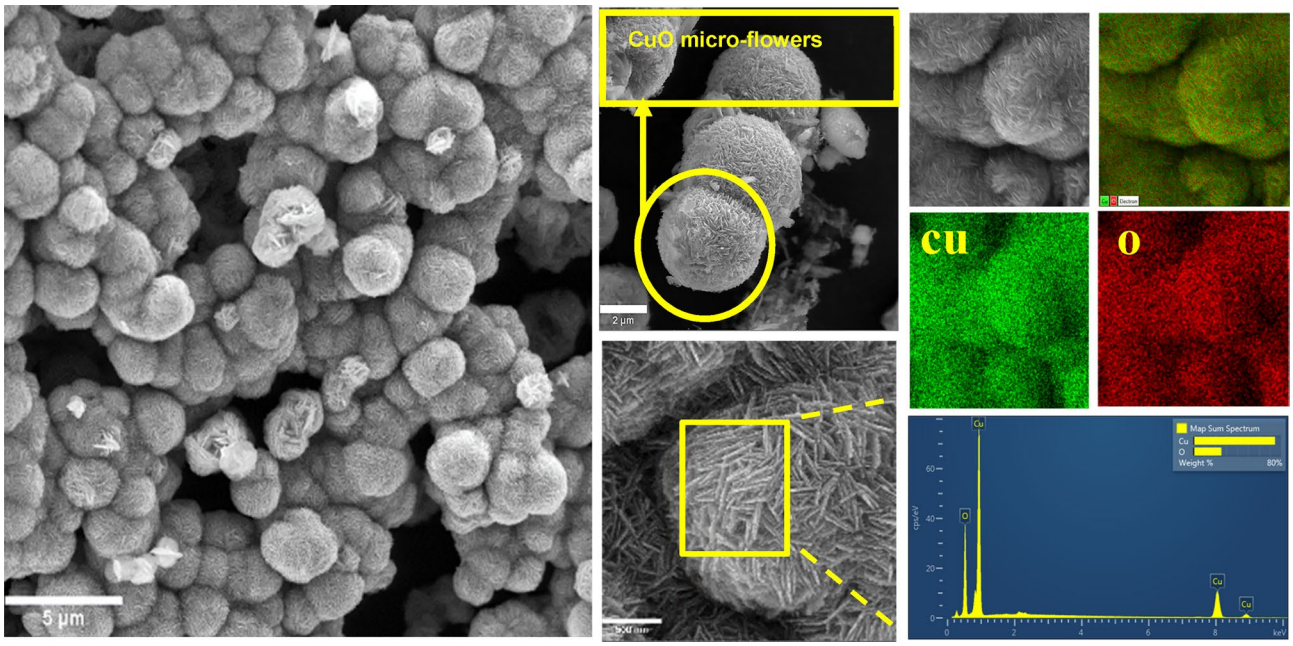

Fig. 4 Low-magnification and high-magnification FESEM, EDS elemental mapping images, and EDX of the synthesized CuO micro-flowers

The microwave-assisted hydrothermal method, which is used, has emerged as a promising approach for synthesizing metal oxide nanostructures, offering a range of benefits. One of the key advantages is the ability to produce nanostructures with fine crystals and controllable morphology. By combining the hydrothermal method with microwave heating, this technique allows for the precise control over the size and shape of metal oxide nanostructures. The result is a high degree of purity and a narrow distribution of grain sizes, which is crucial for many applications. In addition to the refined crystal properties, the microwave hydrothermal method offers rapid synthesis and improved energy efficiency compared to traditional hydrothermal methods. The application of microwave heating reduces the reaction time significantly, enabling the production of metal oxide nanostructures in a shorter duration. Moreover, it reduces energy consumption, making the process more environmentally friendly [34–36].

The morphology and chemical composition of synthesized PPy particles were also studied by FESEM and EDX as depicted in Fig. 5. PPy particles exhibit nonwoven structures composed of nanowires with an average diameter of 30 nm, which were formed using cetyltrimethylammonium bromide (CTAB) as a soft template. CTAB is a cationic surfactant with both hydrophilic and hydrophobic moieties, which can form micelles of various sizes and shapes in aqueous media. The morphology of these micelles and, consequently, the morphology of the synthesized PPy can be controlled by varying the solution's CTAB concentration, temperature, and pH. At specific CTAB concentrations, cylindrical micelles can be formed. By adding pyrrole monomers and ammonium persulfate (APS) to the media, bulk polymerization occurs in the interior of these threadlike micellar aggregates [37, 38]. Figure 6 illustrates the morphology, structure, and chemical composition of CuO/PPy NCs with varying PPy contents (3.5-, 5-, 6.2-, and 8.8-wt% PPy). These high-magnification images indicate that CuO micro-flowers and PPy nanowires are attached in many areas, forming well-distributed composites.

3.6 Electrochemical properties of samples

The composite structure of CuO/PPy NCs renders them an auspicious candidate for energy storage applications. Consequently, the electrochemical performance of these composites was scrutinized as an active anode material for Li-ion batteries. For electrochemical analysis, the synthesized samples were deployed as the working electrode in a 2025 coin-type cell. A lithium sheet was used as the counter and reference electrode, while celgard 2300 was utilized as a separator. The cell electrolyte is composed of LiPF6 (1.0 mol L^{-1}) in a 1:1 (w:w) mixture of ethylene carbonate (EC) and dimethyl carbonate (DMC). The entire cell assembly was conducted in an argon-filled glove box, followed by carrying out cyclic discharge/charge measurements on the prepared coin cells.

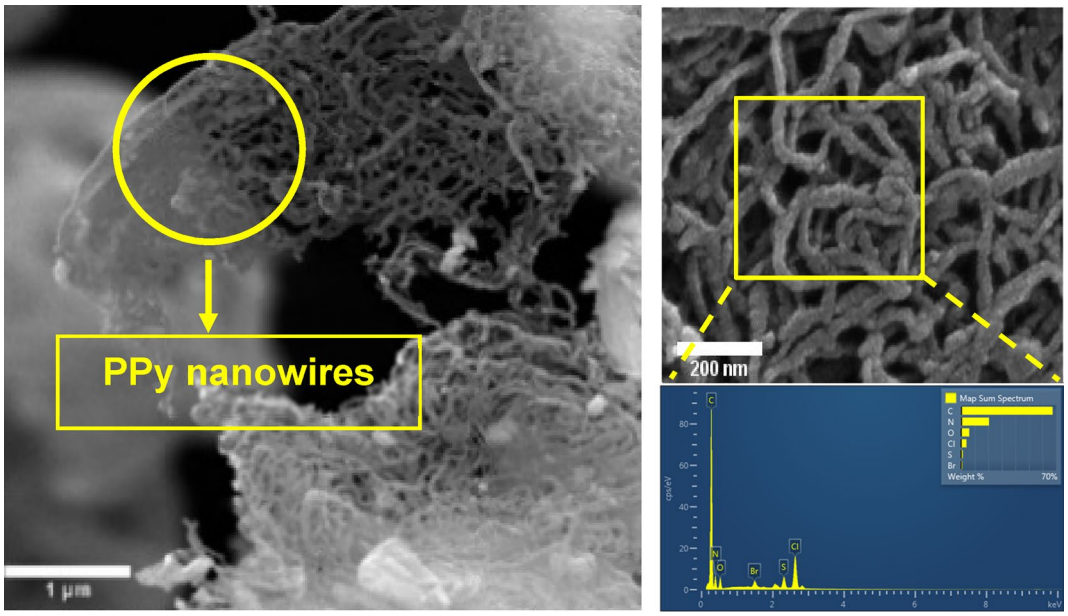

Fig. 5 Low-magnification and high-magnification FESEM and EDX of the synthesized PPy nanowires

3.6.1 Discharge/charge profile

Figure 7 presents the galvanostatic discharge/charge profiles of the anodes composed of bare CuO micro-flowers and CuO/PPy NCs with various concentrations of PPy nanowires (3.5, 5, 6.2, and 8.8 wt%). It can be observed that the discharge–charge profiles of CuO/PPy NCs are analogous to that of bare CuO, indicating that the incorporation of organic polypyrrole does not alter the lithium storage behavior of CuO anodes. Specifically, the initial discharge and charge capacities of bare CuO anode are 1010 and 723 mAh g^{-1}, respectively, at a rate of 0.2C. However, due to the formation of irreversible phases during the first charge process, the second discharge capacity decreased to 769 mAh g^{-1} and gradually dropped to 710 and 630 mAh g^{-1} after the fifth and tenth cycles, respectively.

In the case of CuO/3.5-wt% PPy, as depicted in Fig. 7, the initial discharge and charge capacities are 931 and 670 mAh g^{-1}, respectively, at 0.2 C and decrease to 673, 610, and 526 mAh g^{-1} for the second, fifth, and tenth cycles, respectively. For CuO/5-wt% PPy, the first and second discharge and charge capacities are 944, 676, 667, and 626 mAh g^{-1}, respectively, demonstrating a marginal improvement compared to the CuO/3.5-wt% PPy sample. For CuO/6.2-wt% PPy, the first and second discharge and charge capacities are 943, 652, 627, and 588 mAh g^{-1}, respectively. Lastly, for CuO/8.8-wt% PPy, the initial and second discharge and charge capacities are 915, 718, 688, and 571 mAh g^{-1}, respectively.

3.6.2 Differential capacity versus voltage

To elucidate the redox behavior of the samples, Fig. 8 displays the differential capacity versus voltage (dQ/dV) plots of the first, second, fifth, and tenth cycles for both bare CuO micro-flowers and CuO/PPy NCs with varying PPy weight ratios. The peaks observed in the dQ/dV plots represent the plateaus present in the discharge–charge curves, which correspond to the lithiation and delithiation reactions of the samples. As depicted in Fig. 8, three reduction peaks can be observed in the first discharge curves of all samples. These peaks, located at around 2.1, 1.2, and 0.97 V, respectively, are attributed to the insertion of lithium-ion and the formation of $[Cu^{II}_{1-x}Cu^{I}_{x}]O_{1-x/2}$ $(0 \le x \le 0.4)$ solid solution, the formation of Cu_2O, and the decomposition of Cu_2O into Li_2O and Cu. Furthermore, two oxidation peaks are observed in the first charge curves of all samples, appearing at approximately 2.3 and 2.7 V, respectively, which correspond to the delithiation process $2Cu + Li_2O \rightarrow Cu_2O + 2Li$ and the partial oxidation of Cu_2O into CuO [18, 39, 40].

3.6.3 Cyclic stability of samples

To investigate the impact of PPy nanowires on the cyclic stability and performance of the samples, cyclic discharge and charge were performed for 100 cycles. Figure 9 displays the cyclic performance of CuO/PPy NCs with varying PPy contents, in comparison to pure CuO micro-flowers. It is evident that the cyclic stability of CuO/PPy NCs has been significantly enhanced by increasing the PPy content from 3.5 to 6.2 wt%.

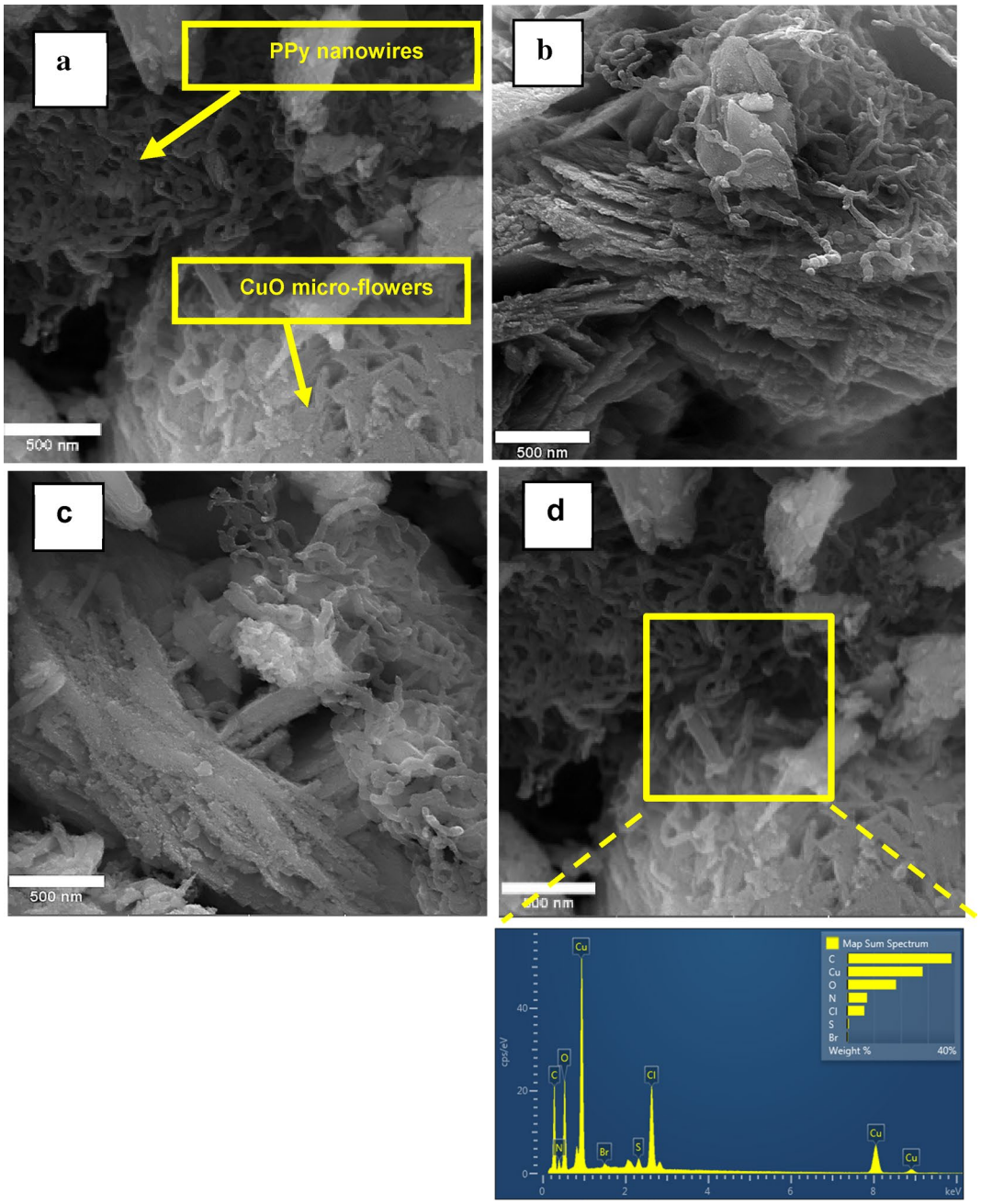

Fig. 6 FESEM images and EDX of the synthesized CuO/3.5-wt% PPy (**a**), CuO/5-wt% PPy (**b**), CuO/6.2-wt% PPy (**c**), and CuO/8.8-wt% PPy (**d**)

Hybrid CuO/PPy NCs exhibit superior cyclic stability as compared to bare CuO micro-flowers. The discharge capacity of CuO micro-flowers was 776 mAh g^{-1} in the second cycle, which decreased to 89 mAh g^{-1} after 100 cycles. Thus, the capacity retention of bare CuO was only 11% (compared to the second cycle). In contrast, CuO/3.5-wt% PPy delivered a second discharge capacity of 678 mAh g^{-1}, which was reduced to 128 mAh g^{-1} after the 100th cycle, with a capacity retention of 18%. Similarly, CuO/5-wt% PPy exhibited second and 100th discharge capacities of 668 mAh g^{-1} and 231 mAh g^{-1}, respectively, with a retention capacity of 34%, demonstrating slight improvement over bare CuO and CuO/3.5-wt% PPy. CuO/6.2-wt% PPy displayed second and 100th discharge capacities of 627 mAh g^{-1} and 371 mAh g^{-1}, respectively, with an optimum retention capacity of 60%, which is five times higher than that of the bare CuO sample, thus demonstrating the best cyclic performance among all synthesized NCs in this work. Furthermore, for CuO/8.8-wt% PPy, the retention capacity reached

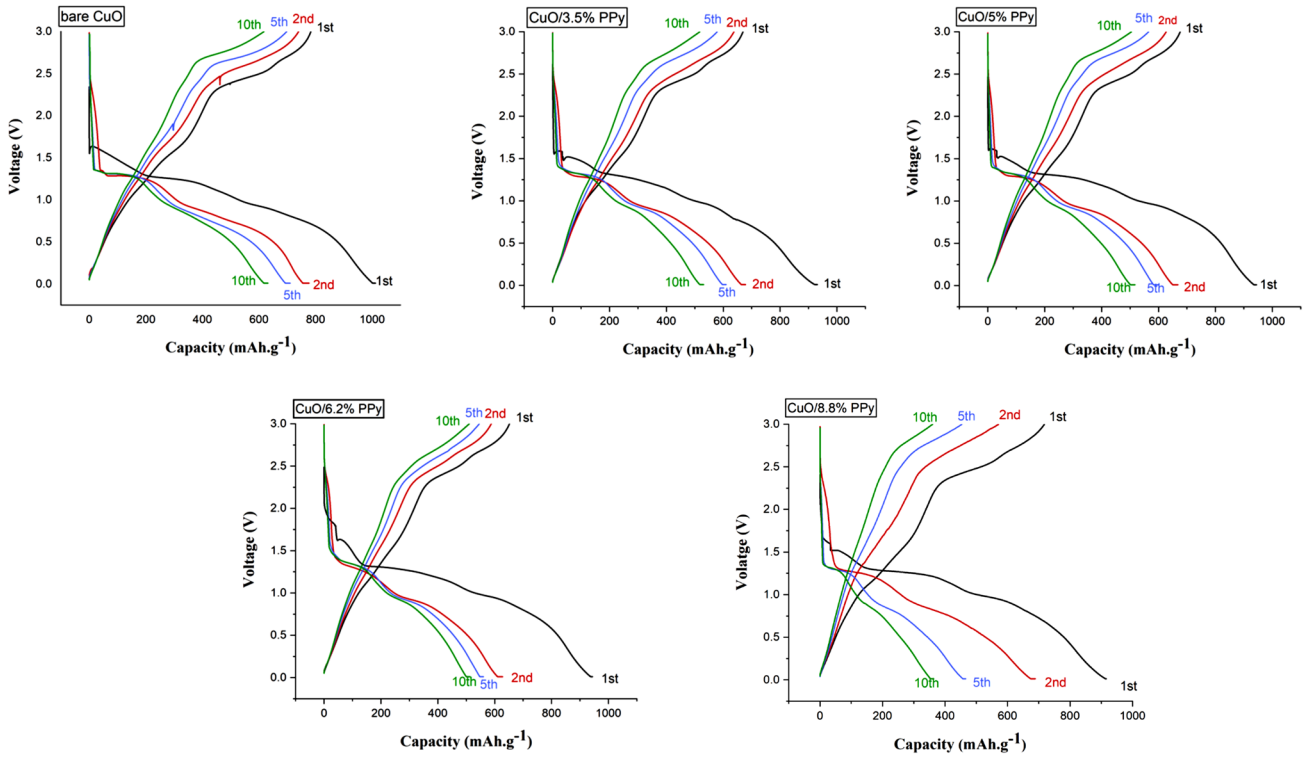

Fig. 7 Discharge/charge curves at different cycles of bare CuO micro-flowers, CuO/3.5-wt% PPy, CuO/5-wt% PPy, CuO/6.2-wt% PPy, and CuO/8.8-wt% PPy

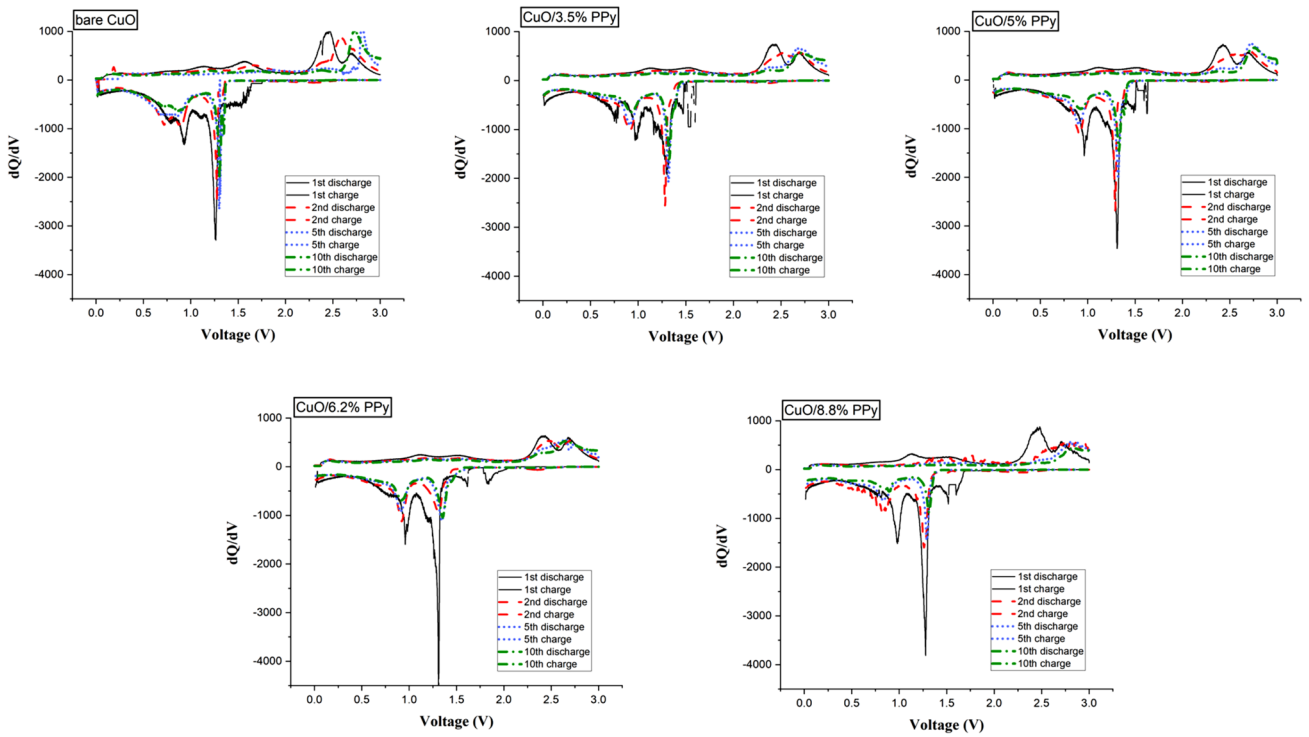

Fig. 8 Differential capacity versus voltage plots of bare CuO micro-flowers, CuO/3.5-wt% PPy, CuO/5-wt% PPy, CuO/6.2-wt% PPy, and CuO/8.8-wt% PPy

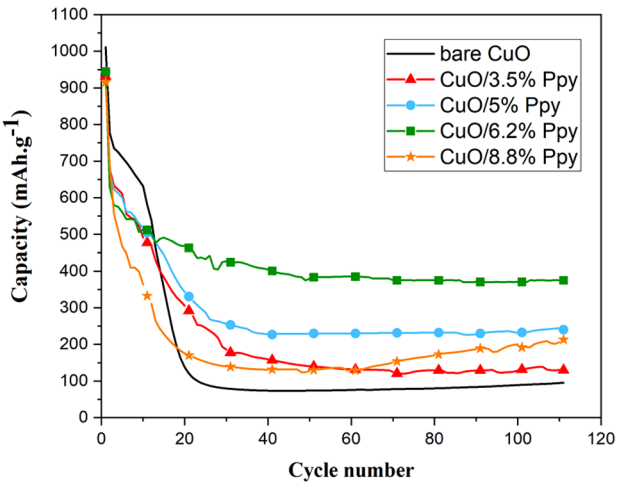

Fig. 9 Comparative cyclic performance of bare CuO micro-flowers and CuO/PPy with different PPy weight ratios

29% with the second and 100th discharge capacities of 688 mAh g^{-1} and 200 mAh g^{-1}, respectively.

The improved performance observed in CuO/PPy NCs anodes, in comparison with bare CuO anode, is primarily attributed to the presence of PPy nanowires, which enable accommodation of volume changes during consecutive discharge–charge processes and prevent the active anode material from pulverization and aggregation, thereby increasing its mechanical integrity[24, 25, 41]. As seen in Fig. 9, the capacity of CuO/8.8-wt% PPy increased gradually after the 50th cycle. This phenomenon is commonly observed for metal oxide active anode materials, and it is likely related to the formation of a Solid Electrolyte Interface (SEI) and activation of the anode material. During consecutive discharge–charge processes, the electrolyte decomposes on the surface of the anode, resulting in the formation of a polymeric gel-like layer on the surface of the anode, known as SEI. This layer contains electroactive compounds, such as lithium carbonate and methoxide, which deliver excess capacity at low potential through pseudo-capacitance-type behavior. At this stage, the decomposition quantity of SEI is greater than its formation during the discharge–charge process, resulting in the thickening of the SEI membrane and generating extra capacity. Moreover, successive discharge and charge cycles cause volume variation in the anode active material and increase available surface and Li^+ diffusion [42, 43].

4 Conclusion

In this study, we have successfully synthesized CuO micro-flowers, PPy nanowires, and CuO/PPy NCs with varying PPy weight ratios. Our results demonstrate that the PPy content plays a critical role in both the structural characteristics and lithium storage properties of the hybrid CuO/PPy NCs. The presence of PPy nanowires serves to accommodate the significant volume changes experienced by CuO structures during the charge and discharge processes. It prevents anode pulverization due to the elastic nature of the polypyrrole. As a result of the formation of organic/inorganic nanocomposites of CuO/PPy NCs, we observe higher lithium storage capacity, better cyclic stability, and higher capacity retention. Specifically, we find that an increase in the weight percentage of polypyrrole leads to a significant improvement in discharge/charge capacities and cycling performance compared to bare CuO micro-flowers. Notably, we identify the optimized CuO/PPy NCs with 6.2-wt% PPy as having a high initial capacity of 943 mAh g^{-1} and retaining a high reversible value of 371 mAh g^{-1} after 100 cycles. These improved performance characteristics can be attributed to the beneficial structural features provided by PPy nanowires.

Author contributions Conceptualization: PV, SMHH, MH, SKS. Methodology: SMHH, MH. Formal analysis and investigation: MH. Writing—original draft preparation: MH. Writing—review, and editing: SKS, MH, PV. Resources: SKS. Supervision: SKS. All authors read and approved the final manuscript.

Declarations

Competing interests The authors declare no competing interests.

References

1. Cheng F, Liang J, Tao Z, Chen J (2011) Functional materials for rechargeable batteries. Adv Mater 23(15):1695–1715
2. Espinoza VS, Erbis S, Pourzahedi L, Eckelman MJ, Isaacs JA (2014) Material flow analysis of carbon nanotube lithium-ion batteries used in portable computers. ACS Sustain Chem Eng 2(7):1642–1648
3. Jin L, Qiu Y, Deng H, Li W, Li H, Yang S (2011) Hollow $CuFe_2O_4$ spheres encapsulated in carbon shells as an anode material for rechargeable lithium-ion batteries. Electrochim Acta 56(25):9127–9132
4. Jiang Y, Jiang Z, Jiang Z, Liu M (2018) Phase and morphology evolution induced lithium storage capacity enhancement of porous CoO nanowires intertwined with reduced graphene oxide nanosheets. ChemElectroChem 5(23):3679–3687
5. Zhang Q et al (2014) CuO nanostructures: synthesis, characterization, growth mechanisms, fundamental properties, and applications. Prog Mater Sci 60:208–337
6. Ding Y, Yang Y, Shao H (2012) Synthesis and characterization of nanostructured $CuFe_2O_4$ anode material for lithium ion battery. Solid State Ionics 217:27–33
7. Hou Q et al (2019) Encapsulation of Fe_2O_3/NiO and Fe_2O_3/Co_3O_4 nanosheets into conductive polypyrrole for superior lithium ion storage. Electrochim Acta 296:438–449
8. Cheng Y-W et al (2018) Freestanding three-dimensional CuO/NiO core–shell nanowire arrays as high-performance lithium-ion battery anode. Sci Rep 8(1):18034

9. Wang C, Xu J, Ma R, Yuen M-F (2014) Facile synthesis of CuO nanoneedle electrodes for high-performance lithium-ion batteries. Mater Chem Phys 148(1–2):411–415
10. Pal J, Mondal C, Sasmal AK, Ganguly M, Negishi Y, Pal T (2014) Account of nitroarene reduction with size-and facet-controlled CuO–MnO_2 nanocomposites. ACS Appl Mater Interfaces 6(12):9173–9184
11. Zhang X et al (2018) Room-temperature vertically-aligned copper oxide nanoblades synthesized by electrochemical restructuring of copper hydroxide nanorods: an electrode for high energy density hybrid device. J Power Sour 383:124–132
12. Chen Z et al (2019) Ultrafine CuO nanoparticles decorated activated tube-like carbon as advanced anode for lithium-ion batteries. Electrochim Acta 296:206–213
13. Wang C et al (2014) Morphology-dependent performance of CuO anodes via facile and controllable synthesis for lithium-ion batteries. ACS Appl Mater Interfaces 6(2):1243–1250
14. Oh SW, Bang HJ, Bae YC, Sun Y-K (2007) Effect of calcination temperature on morphology, crystallinity and electrochemical properties of nano-crystalline metal oxides (Co_3O_4, CuO, and NiO) prepared via ultrasonic spray pyrolysis. J Power Sour 173(1):502–509
15. Xiang JY, Tu JP, Zhang L, Zhou Y, Wang XL, Shi SJ (2010) Self-assembled synthesis of hierarchical nanostructured CuO with various morphologies and their application as anodes for lithium ion batteries. J Power Sources 195(1):313–319
16. Morales J, Sánchez L, Martín F, Ramos-Barrado JR, Sánchez M (2004) Nanostructured CuO thin film electrodes prepared by spray pyrolysis: a simple method for enhancing the electrochemical performance of CuO in lithium cells. Electrochim Acta 49(26):4589–4597
17. Park JC, Kim J, Kwon H, Song H (2009) Gram-scale synthesis of Cu_2O nanocubes and subsequent oxidation to CuO hollow nanostructures for lithium-ion battery anode materials. Adv Mater 21(7):803–807
18. Gao XP et al (2004) Preparation and electrochemical performance of polycrystalline and single crystalline CuO nanorods as anode materials for Li ion battery. J Phys Chem B 108(18):5547–5551
19. Moakhar RS et al (2020) One-pot microwave synthesis of hierarchical C-doped CuO dandelions/g-C3N4 nanocomposite with enhanced photostability for photoelectrochemical water splitting. Appl Surf Sci 530:147271
20. Huang XH, Tu JP, Xia XH, Wang XL, Xiang JY (2008) Nickel foam-supported porous NiO/polyaniline film as anode for lithium ion batteries. Electrochem Commun 10(9):1288–1290
21. Liu R, Duay J, Lee SB (2010) Redox exchange induced MnO_2 nanoparticle enrichment in poly (3, 4-ethylenedioxythiophene) nanowires for electrochemical energy storage. ACS Nano 4(7):4299–4307
22. Sun X, Zhang H, Zhou L, Huang X, Yu C (2016) Polypyrrole-coated zinc ferrite hollow spheres with improved cycling stability for lithium-ion batteries. Small 12(27):3732–3737
23. Wu L et al (2019) PPy-encapsulated SnS_2 nanosheets stabilized by defects on a TiO_2 support as a durable anode material for lithium-ion batteries. Angew Chemie 131(3):821–825
24. Yin Z, Ding Y, Zheng Q, Guan L (2012) CuO/polypyrrole core–shell nanocomposites as anode materials for lithium-ion batteries. Electrochem Commun 20:40–43
25. Yin Z, Fan W, Ding Y, Li J, Guan L, Zheng Q (2015) Shell structure control of PPy-modified CuO composite nanoleaves for lithium batteries with improved cyclic performance. ACS Sustain Chem Eng 3(3):507–517
26. Feng L et al (2020) Preparation of CuO@ PPy hybrid nanomaterials as high cyclic stability anode of lithium-ion battery. Micro Nano Lett 15(7):441–445
27. Batool A, Kanwal F, Imran M, Jamil T, Siddiqi SA (2012) Synthesis of polypyrrole/zinc oxide composites and study of their structural, thermal and electrical properties. Synth Met 161(23–24):2753–2758
28. Zhao J, Zhang S, Liu W, Du Z, Fang H (2014) Fe3O4/PPy composite nanospheres as anode for lithium-ion batteries with superior cycling performance. Electrochim Acta 121:428–433
29. Zou G, Li H, Zhang D, Xiong K, Dong C, Qian Y (2006) Well-aligned arrays of CuO nanoplatelets. J Phys Chem B 110(4):1632–1637
30. Wang B, Wu X-L, Shu C-Y, Guo Y-G, Wang C-R (2010) Synthesis of CuO/graphene nanocomposite as a high-performance anode material for lithium-ion batteries. J Mater Chem 20(47):10661–10664
31. Zhou Y et al (2019) Evaporation induced uniform polypyrrole coating on CuO arrays for free-standing high lithium storage anode. J Solid State Electrochem 23(6):1829–1836
32. Cho G, Fung BM, Glatzhofer DT, Lee J-S, Shul Y-G (2001) Preparation and characterization of polypyrrole-coated nanosized novel ceramics. Langmuir 17(2):456–461
33. Thommes M et al (2015) Physisorption of gases, with special reference to the evaluation of surface area and pore size distribution (IUPAC Technical Report). Pure Appl Chem 87(9–10):1051–1069
34. Yang C, Xiao F, Wang J, Su X (2015) 3D flower-and 2D sheet-like CuO nanostructures: microwave-assisted synthesis and application in gas sensors. Sensors Actuators B Chem 207:177–185
35. Volanti DP et al (2008) Synthesis and characterization of CuO flower-nanostructure processing by a domestic hydrothermal microwave. J Alloys Compd 459(1–2):537–542
36. Yang G, Park S-J (2019) Conventional and microwave hydrothermal synthesis and application of functional materials: a review. Materials (Basel) 12(7):1177
37. Rangel-Yagui CO, Pessoa-Jr A, Blankschtein D (2004) Two-phase aqueous micellar systems: an alternative method for protein purification. Brazilian J Chem Eng 21(4):531–544
38. Dai T, Yang X, Lu Y (2006) Controlled growth of polypyrrole nanotubule/wire in the presence of a cationic surfactant. Nanotechnology 17(12):3028
39. Yin Z, Zheng Q (2012) Controlled synthesis and energy applications of one-dimensional conducting polymer nanostructures: an overview. Adv Energy Mater 2(2):179–218
40. Xiang JY, Tu JP, Zhang J, Zhong J, Zhang D, Cheng JP (2010) Incorporation of MWCNTs into leaf-like CuO nanoplates for superior reversible Li-ion storage. Electrochem Commun 12(8):1103–1107
41. Vahdatkhah P, Sadrnezhaad SK, Voznyy O (2022) On the functionality of the polypyrrole nanostructures for surface modification of Co-free Li-rich layered oxide cathode applied in lithium-ion batteries. J Electroanal Chem 914:116317
42. Park S-K, Choi JH, Kang YC (2018) Unique hollow NiO nanooctahedrons fabricated through the Kirkendall effect as anodes for enhanced lithium-ion storage. Chem Eng J 354:327–334
43. Wang Y et al (2020) Cu/Cu2O@ Ppy nanowires as a long-life and high-capacity anode for lithium ion battery. Chem Eng J 391:123597